Journal of the Korean Physical Society (2022) 81:133–138
https://doi.org/10.1007/s40042-022-00498-8

Online ISSN 1976-8524
Print ISSN 0374-4884

ORIGINAL PAPER - CONDENSED MATTER

Strain dependent magnetic properties of 1T-VSe_2 monolayer

Jicheol Son[1] · Brahim Marfoua[1] · Jisang Hong[1]

Received: 18 March 2022 / Revised: 11 April 2022 / Accepted: 12 April 2022 / Published online: 17 May 2022

Abstract
Using the first principles calculations, we investigated the strain dependent magnetic properties of the 1T-VSe_2 monolayer (up to ± 3%). We obtained a metallic band structure, and this feature was preserved under both compressive and tensile strain. The pristine system had a magnetic moment of 0.9 μ_B/unit cell and decreased to 0.68 μ_B /unit cell under − 3% compressive strain whereas it was increased to 1.03 μ_B/unit cell under + 3% tensile strain. The 1T-VSe_2 monolayer had an in-plane magnetic anisotropy with a value of − 0.48 meV/cell. The in-plane anisotropy features were maintained in both compressive and tensile strains. The orbital resolved magnetic anisotropy indicated that the V atom contributed to the perpendicular magnetic anisotropy while the Se atom had an in-plane anisotropy. We found that the Se dominated the anisotropy. We also calculated the temperature dependent Curie temperature (T_C). The pristine structure had a T_C of 260 K, and the strain effect enhanced the T_C. Particularly, the compressive strain affected further the exchange parameter resulting in substantial enhancement of the Curie temperature where a T_C of 570 K was achieved at − 3% strain. Our finding regarding the strained VSe_2 could help for further investigation in spintronics and straintronics applications.

Keywords VSe2 · Strain

1 Introduction

Two-dimensional (2D) materials have attracted extensive investigation efforts in condensed matter physics and materials sciences owing to their intriguing physical properties not found in bulk or macroscopic materials. Indeed, 2D materials may have outstanding potential innovative device applications such as electronics, optoelectronics, valleytronics, or straintronics. To date, numerous types of 2D materials have been investigated either theoretically or experimentally. Nonetheless, most of the previously reported 2D materials are non-magnetic [1–6]. This non-magnetic feature may hinder the expansion of spintronics applications in the 2D material system. Thus, it is highly desirable to find new 2D materials which exhibit an intrinsic ferromagnetic (FM) ordering. Thus, searching for 2D materials nowadays become one of the most active research issues in 2D materials sciences and condensed matter physics.

Since the key factor for real spintronics applications is the room temperature FM state, probing room temperature 2D materials becomes one of the most intriguing issues. To this end, several theoretical first principles calculations proposed quite a lot of materials that can display room temperature or even higher Curie temperature (T_C) [7–9]. However, limited 2D FM materials were experimentally fabricated in atomic scale thickness so far despite these theoretical predictions. In this regard, the most well-known fabricated 2D magnetic materials are Fe_3GeTe_2, CrI_3, and $CrGeTe_3$ [10–12]. For instance, the 2D single-layer Fe_3GeTe_2 layer shows a metallic state with a Curie temperature of 130 K and it has a uniaxial anisotropy of 2.76 meV/cell [10, 13]. In contrast, both CrI_3 and $CrGeTe_3$ display semiconducting behavior, and their Curie temperatures (~ 30–45 K) are rather low compared with that of the Fe_3GeTe_2. Also, the metallic monolayer $CrBr_3$ was successfully synthesized and a spontaneous magnetization was confirmed with a T_C of 34 K [14]. Nevertheless, we note that all these materials have relatively low Curie temperature.

Interestingly, some 2D FM transition metal dichalcogenide (TMD) systems have been recently exfoliated with relatively larger T_C such as $CrTe_2$ few layers films (7 layers) which show metallic character with a T_C up to 300 K[15].

✉ Jisang Hong
hongj@pknu.ac.kr

[1] Department of Physics, Pukyong National University, Busan 48513, Korea

In addition, room temperature FM was observed in the monolayer limit of the metallic manganese selenide ($MnSe_x$) films [16]. Remarkably, a single-layer VSe_2 structure was experimentally grown from the bulk crystal and exhibiting room temperature ferromagnetism with a metallic state [17, 18]. On the theoretical side, Popov et al. found that the VSe_2 monolayer may have either 2H or 1T phase depending on the Hubbard (U) correction term[19]. In addition, the charge density wave (CDW) phase may appear in the VSe_2 monolayer owing to the Fermi surface nesting. Nonetheless, due to the extreme dependence on the experimental environment such as the nature of the growth substrate, the charge-ordering transition in the monolayer VSe_2 is still under debate[20]. Indeed, many theoretical studies focused on the 2H-VSe_2 monolayer structure [21, 22]. However, unlike the extensive investigations on the 2H phase, it is rare to find studies on the physical properties of the 1T-VSe_2 monolayer. On the other hand, strain engineering can be a practical approach to control the magnetic properties of 2D materials for promising spintronic applications. Thus, in this report, we will explore the magnetic properties and also the strain dependent magnetic properties of the 1T VSe_2 monolayer. Particularly, we will investigate the effect of the biaxial tensile and compressive strain (ranging from 1 to 3%) on the magnetic properties and Curie temperature (T_C).

2 Numerical method

To calculate the electronic structure and magnetic properties, the Vienna ab initio simulation package (VASP) [23, 24] was employed using the projector augmented wave (PAW) method [24, 25]. We selected the Perdew-Burke-Ernzerhof (PBE) with generalized gradient approximation (GGA) as an exchange–correlation potential[26] combined with the effective on-site Coulomb interactions with the Hubbard parameters of $U = 2$ eV and $J = 0.84$ eV [27–29] for the 3d orbital of the V element [30, 31]. A plane wave energy cutoff of 650 eV was used for all the calculations. Also, a slab geometry was considered with a vacuum distance of more than 20 Å, and this is to avoid an artificial interaction with the neighboring unit cell. The residual force on each atom was lesser than 0.01 eV/Å and the energy convergence was smaller than 10^{-6} eV for geometry optimization with a sampled k-point mesh of $13 \times 13 \times 1$. To find the magnetic anisotropy energy, a non-collinear spin configuration with spin–orbit coupling was considered, and a dense k-mesh of $21 \times 21 \times 1$ was used in all systems for accuracy checking. To estimate the Curie temperature (T_C), we considered the Metropolis Monte Carlo (MC) simulations using the VAMPIRE software package[32, 33] to calculate the temperature dependent magnetization curve.

3 Numerical results

The 1T-VSe_2 monolayer is a transition metal dichalcogenides (TMDs) system structured in a hexagonally packed plane of the form Se–V–Se with octahedral prismatic coordination. To find the equilibrium lattice constant, we performed the full structure relaxation without any constraint, and obtained the lattice parameters of $a = b = 3.344$ Å. Figure 1a–b shows the top and side view of the optimized 1T-VSe_2 monolayer structure without any strain. The red color represents the V atom while the Se atom is represented by the green color. To calculate the total energy difference between ferromagnetic (FM) and antiferromagnetic (AFM) states ($E_{diff} = E_{AFM} - E_{FM}$), we used a 2×2 supercell unit cell. We found that the FM ground state was favored with an energy difference of 15 meV/unit cell, and the calculated magnetic moment was 0.90 μ_B/unit cell. Based on this 1T pristine structure, we applied both compressive and tensile strains (up to $\pm 3\%$). Here, we allowed the full atomic relaxation. We found that the FM ground state was further enhanced in both compressive and tensile strains as shown in Table 1. For instance, the energy difference was increased to 19 meV/unit cell and 33 meV/unit cell with the compressive (-3%) and tensile (3%) strains. Also, we present the strain dependent magnetic moment in Table 1. The magnetic moment decreased with compressive strain, where it was 0.68 μ_B/unit cell at -3% while it showed the reversed behavior with the tensile strain and attained the value of 1.03 μ_B/unit cell at 3%. Indeed, the major contribution to the magnetic moment stems from the V atom, but the Se also has a small induced magnetic moment. For instance, the V had 1.10 μ_B while the Se had -0.1 μ_B in the pristine system (0%). Since the 1T-VSe_2 monolayer had an FM ground state under strain, we only focus on the FM state.

Figure 2 shows the strain dependent spin polarized band structure. The black and red colors represent the majority and minority spin bands. As shown in Fig. 2a, the calculated band structure without any strain has a normal metallic state. Since the central issue of this report is to explore the strain dependent magnetic properties, we applied both compressive

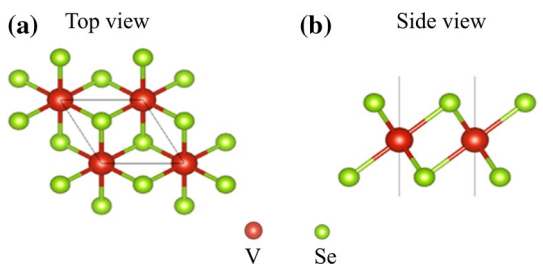

Fig. 1 **a**Top view and **b** side view 1-T VSe_2 monolayer. The red color represents the V atom and the green color indicates the Se atom

Table 1 Calculated strain dependent total energy difference (E_{AFM}–E_{FM}), total magnetic moment ($m_{unitcell}$), V magnetic moment (m_V), Se magnetic moment (m_{Se}) magnetocrystalline anisotropy energy (MAE), and J exchange parameter of the 1T-VSe_2

		Compressive strain			Tensile strain		
	Pristine 1T-VSe_2	−1%	−2%	−3%	1%	2%	3%
E_{AFM}–E_{FM} (meV/unitcell)	15	16	18	19	19	26	33
$m_{unitcell}$ (μB)	0.90	0.81	0.74	0.68	0.98	1.02	1.03
m_V (μB)	1.10	0.99	0.89	0.80	1.21	1.27	1.30
m_{Se} (μB)	− 0.10	− 0.09	− 0.07	− 0.06	− 0.12	− 0.13	− 0.13
MAE (meV/unitcell)	− 0.48	− 0.32	− 0.22	–0.15	− 0.57	− 0.59	− 0.57

and tensile strains up to ± 3%. As an illustration, we present in Fig. 2b the band structure with the compressive strain of − 3% and Fig. 2c with the tensile strain of + 3%. With compressive strain, the exchange splitting was suppressed. We also found that the minority spin bands shifted downward whereas the majority spin band moved upward relative to the Fermi level. In contrast, under the tensile strain, the exchange splitting was further enhanced. Besides, the minority spin band moved upward while the majority spin band shifted downward with respect to the Fermi level. Consequently, the magnetic moment was suppressed with compressive strain while it was enhanced under tensile strain.

We now discuss magnetocrystalline anisotropy. We performed a non-collinear total energy calculation including the spin–orbit coupling along [001] and [100] directions. Here, the magnetic anisotropy energy (MAE) is defined as $E_{MAE} = E_{100} - E_{001}$. In Tabel 1 we present the strain dependent MAE. The pristine layer had an in-plane magnetic anisotropy and the calculated magnetic anisotropy was − 0.48 meV/unit cell. The in-plane anisotropy was still preserved in both compressive and tensile strains, but it had different strain dependencies. With increasing the compressive strain, the in-plane magnetic anisotropy was gradually decreased. In contrast, the in-plane anisotropy was insensitive to the tensile strain because the variation of the magnetic anisotropy energy was rather weak. Unlike the magnetic moment which is based on the difference in the number of electrons in both spin states, the magnetic anisotropy stems from the spin–orbit coupling (SOC) effect. Hence, the MAE is strongly sensitive to the orbital characters in both occupied and unoccupied spin states because the direction of magnetization is coupled through the angular momentum operator. Since the straightforward analysis of MAE is not an easy task, one may refer to the second-order perturbation theory for semi-quantitative understanding [34], and the MAE is expressed in the below

$$MAE = \xi^2 \sum_{u,o;\alpha,\beta} (2\delta_{\alpha\beta} - 1) \left[\frac{|< u,\alpha|\hat{L}z|o,\beta >|^2 - |< u,\alpha|\hat{L}x|o,\beta >|^2}{\varepsilon_{u,\alpha} - \varepsilon_{o,\beta}} \right], \quad (1)$$

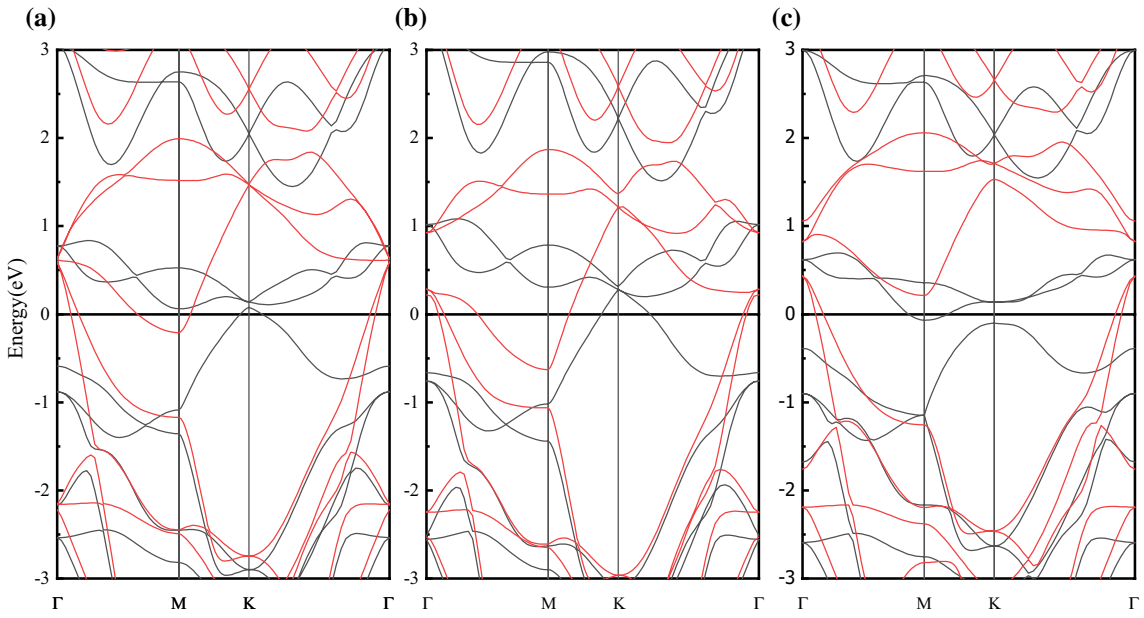

Fig. 2 Calculated spin polarized band structure of VSe_2 at **a** 0% pristine VSe_2, **b** − 3% compressive strain, **c** 3% tensile strain. The black color represents the majority while the red color denotes the minority spin bands

where ξ is the strength of the SOC and $\varepsilon_{u,\alpha}(\varepsilon_{o,\beta})$ is the energy level of unoccupied (occupied) states with spin α (β). Indeed, the orbital anisotropy and magnetization direction are strongly correlated in the second-order perturbation theory, and the details are presented in elsewhere [35]. For quantitative understanding, we calculated the strain dependent orbital resolved magnetic anisotropy of Se and V atoms at 0, − 3, and 3% as shown in Fig. 3a–f. In the pristine system, the Se atom induced an in-plane anisotropy.

Note that the magnetic moment itself of the Se atom is much smaller than that of the V atom, but the Se atom dominated the contribution to the magnetic anisotropy because it has a heavier atomic mass compared to the V atom resulting in strong SOC. Overall, we obtained an in-plane anisotropy. Under compressive strain, the in-plane is still preserved. However, both contributions from Se and V atoms are substantially suppressed compared with that in the pristine system. Therefore, the overall in-plane anisotropy was decreased. For tensile strain, the in-plane anisotropy from the Se atom was enhanced, but at the same time, the perpendicular contribution from the V atom was also enhanced. This opposite behavior canceled the net effect, and consequently, the tensile strain did not strongly affect the in-plane anisotropy compared with that in the pristine system.

We also calculated the strain dependent Curie temperature (T_C). The Curie–Weiss mean field theory [36] is the most straightforward approach to calculate the critical temperature. However, this molecular mean field theory usually overestimates the Curie temperature [37]. Thus, we calculated the Curie temperature using Metropolis Monte Carlo (MC) simulations. Here, the temperature dependent magnetization curve was calculated using 10,000 equilibration steps and 10,000 averaging steps using the VAMPIRE software package [32, 33]. According to the spin Heisenberg model with the magnetic anisotropy factor, the Hamiltonian equation is given as

$$\hat{H} = -\sum_{i,j} J\hat{m}_i \cdot \hat{m}_j - k_2 \sum_i m_z^2, \tag{2}$$

where $\hat{m}_i$ and $\hat{m}_j$ are the magnetic moments (in μ_B) at sites i and j, k_2 represents the anisotropy constant whereas m_z is the spins pointing along a single preferred axis (known as the

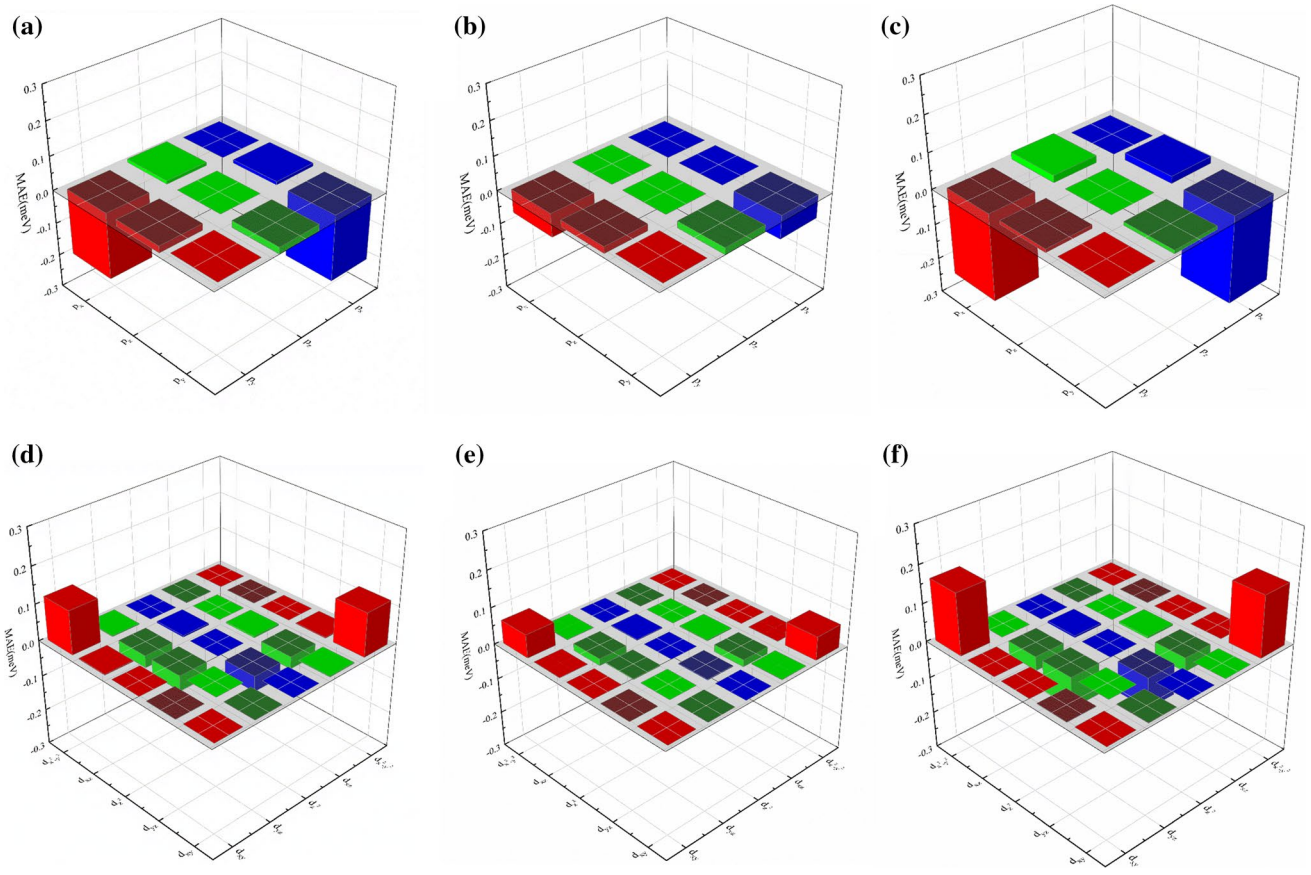

Fig. 3 SOC resolved MAE of the Se atom at **a** 0% pristine VSe_2, **b** − 3% compressive strain, **c** 3% tensile strain. SOC resolved MAE of the V atom at **d** 0% pristine VSe_2, **e** − 3% compressive strain, **f** 3% tensile strain

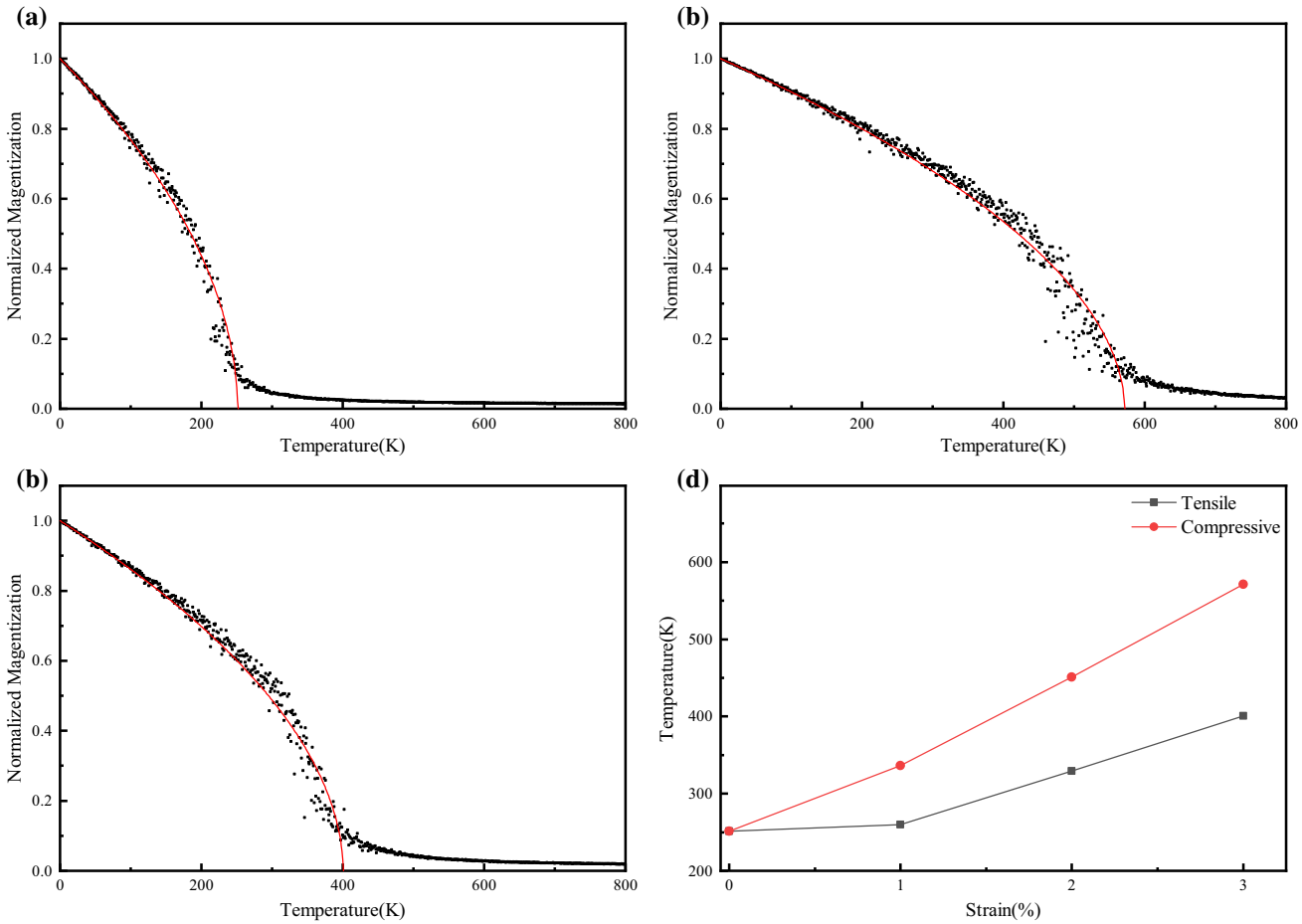

Fig. 4 Temperature dependent magnetization curves for **a** 0% pristine VSe_2, **b** − 3% compressive strain, and **c** 3% tensile strain. **d** Strain dependent Curie temperature of the VSe_2 at $0, \pm 1, \pm 2, \pm 3\%$ strain

easy axis), and J is the exchange parameter. The exchange parameter J was obtained using the relation $J = \frac{E_{ex}}{Nm^2}$. Here N is the number of magnetic atoms per cell. We considered a supercell of 50×50 with periodic boundary conditions in the MC simulations to reduce the finite-size effects. As an illustration, Fig. 4a–c shows the temperature dependent magnetization curve for both pristine and strained structures ($\pm 3\%$). Note that Fig. 4d shows the strain dependent Curie temperature at $0, \pm 1, \pm 2, \pm 3\%$ strain. Here, the temperature-dependent magnetization curve was fitted using the Curie-Bloch equation in the classical limit as given below

$$m(T) = \left[1 - \frac{T}{T_C}\right]^{\beta}, \tag{3}$$

where T is the temperature and T_C is the Curie temperature. The calculated critical exponent β was 0.53 in the pristine. Meanwhile, it became 0.52 up to − 3% compressive strain and 0.51 at 3% tensile strain. The pristine structure had the Curie temperature of 260 K and this is close to the experimentally reported value [17]. Interestingly, substantial enhancement was found in the compressive strain because the estimated Curie temperature was increased to 570 K at − 3% compressive strain. While we found that the Curie temperature was enhanced to 400 K in 3% tensile strains. Indeed, the compressive strain had more strongly affected the exchange parameter, and this resulted in the substantially enhanced Curie temperature of the compressive strained system.

4 Conclusion

In summary, we systematically investigated the strain dependent magnetic properties of 1T-VSe_2 monolayer (up to $\pm 3\%$). The 1T-VSe_2 had a ferromagnetic ground state with a metallic state. The FM ground state was preserved in both compressive and tensile strain. The magnetic moment was 0.9 μ_B/unit cell in the pristine system and reduced to 0.68 μ_B/unit cell under the compressive strain of − 3%. Whereas the opposite behavior was found under the tensile strain (3%) reaching the value of 1.03 μ_B/unit cell. Also, the metallic band feature was maintained under both compressive and tensile strain. We found that the minority spin band was

influenced by the compressive strain, but the majority spin band was affected by the tensile strain. We obtained an in-plane MAE of − 0.48 meV/unit cell in the pristine system. The in-plane magnetic anisotropy was preserved in both compressive and tensile strains but showed different tendencies. For instance, the in-plane magnetic anisotropy was suppressed under compressive strain while it was almost unchanged under tensile strain. The orbital resolved magnetic anisotropy revealed that the V atom contributed to the perpendicular magnetic anisotropy while the Se atom had an in-plane anisotropy. We found that the Se contribution dominated the magnetic anisotropy. Using the Metropolis Monte Carlo (MC) simulations, we obtained a Curie temperature of 260 K by calculating the temperature dependent magnetization curve and this value is close to the experimental reported one. Under the compressive and tensile strain, the Curie temperature was enhanced. Though the compressive strain affected further the exchange parameter resulting in substantial enhancement of the Curie temperature where a T_C of 570 K was achieved at − 3% strain. Overall, our study proposes that the Curie temperature of the 1T-VSe_2 monolayer could be enhanced under the biaxial strain implying potential applications in spintronics and straintronics.

Acknowledgements This work was supported by the National Research Foundation of Korea(NRF) grant funded by the Korea gove rnment(MSIT) (2022R1A2C1004440).

References

1. R.R. Nair, P. Blake, A.N. Grigorenko, K.S. Novoselov, T.J. Booth, T. Stauber, N.M. Peres, A.K. Geim, Science **320**, 1308 (2008)
2. D. Kim, A. Hashmi, C. Hwang, J. Hong, Surf. Sci. **610**, 27 (2013)
3. S. Tongay, J. Zhou, C. Ataca, K. Lo, T.S. Matthews, J. Li, J.C. Grossman, J. Wu, Nano Lett. **12**, 5576 (2012)
4. L. Li, Y. Yu, G.J. Ye, Q. Ge, X. Ou, H. Wu, D. Feng, X.H. Chen, Y. Zhang, Nat. Nanotechnol. **9**, 372 (2014)
5. T. Dietl, H. Ohno, Rev. Mod. Phys. **86**, 187 (2014)
6. D.D. Awschalom, M.E. Flatté, Nat. Phys. **3**, 153 (2007)
7. K. Zhao, Q. Wang, Appl. Surf. Sci. **505**, 144620 (2020)
8. Z. Jiang, P. Wang, X. Jiang, J. Zhao, Nanoscale. Horiz. **3**, 335 (2018)
9. Y. Hu, X. Liu, Z. Shen, Z. Luo, Z. Chen, X. Fan, Nanoscale **12**, 11627 (2020)
10. Z. Fei et al., Nat. Mater. **17**, 778 (2018)
11. C. Gong et al., Nature **546**, 265 (2017)
12. B. Huang et al., Nature **546**, 270 (2017)
13. H.L. Zhuang, P. Kent, R.G. Hennig, Phys. Rev. B **93**, 134407 (2016)
14. Z. Zhang, J. Shang, C. Jiang, A. Rasmita, W. Gao, T. Yu, Nano Lett. **19**, 3138 (2019)
15. X. Zhang et al., Nat. Commun. **12**, 1 (2021)
16. D.J. O'Hara et al., Nano Lett. **18**, 3125 (2018)
17. M. Bonilla et al., Nat. Nanotechnol. **13**, 289 (2018)
18. W. Yu et al., Adv. Mater. **31**, 1903779 (2019)
19. Z. Popov, N. Mikhaleva, M. Visotin, A. Kuzubov, S. Entani, H. Naramoto, S. Sakai, P. Sorokin, P. Avramov, PCCP **18**, 33047 (2016)
20. G. Duvjir, B.K. Choi, T.T. Ly, N.H. Lam, K. Jang, D.D. Dung, Y.J. Chang, J. Kim, Nanotechnology **32**, 364002 (2021)
21. J. Liu, W.-J. Hou, C. Cheng, H.-X. Fu, J.-T. Sun, S. Meng, J. Phys: Condens. Matter **29**, 255501 (2017)
22. H. Pan, J. Phys. Chem. C. **118**, 13248 (2014)
23. G. Kresse, J. Furthmüller, Phys. Rev. B **54**, 11169 (1996)
24. G. Kresse, D. Joubert, Phys. Rev. B **59**, 1758 (1999)
25. P. Blochl, Phys. Rev. B **50**, 17953 (1994)
26. J.P. Perdew, K. Burke, M. Ernzerhof, Phys. Rev. Lett. **77**, 3865 (1996)
27. S. Dudarev, G. Botton, S. Savrasov, C. Humphreys, A. Sutton, Phys. Rev. B **57**, 1505 (1998)
28. A. Liechtenstein, V. Anisimov, J. Zaanen, Phys. Rev. B **52**, R5467 (1995)
29. V.I. Anisimov, F. Aryasetiawan, A. Lichtenstein, J. Phys: Condens. Matter **9**, 767 (1997)
30. H.-R. Fuh, C.-R. Chang, Y.-K. Wang, R.F. Evans, R.W. Chantrell, H.-T. Jeng, Sci. Rep. **6**, 32625 (2016)
31. Z. Guan, S. Ni, Nanoscale **12**, 22735 (2020)
32. R.F. Evans, W.J. Fan, P. Chureemart, T.A. Ostler, M.O. Ellis, R.W. Chantrell, J. Phys: Condens. Matter **26**, 103202 (2014)
33. R. Evans. URL http://vampire.york.ac.uk (2016)
34. D.-S. Wang, R. Wu, A. Freeman, Phys. Rev. B **47**, 14932 (1993)
35. I. Khan, J. Hong, J. Korean Phys. Soc. **72**, 1343 (2018)
36. J. S. Smart. Effective field theories of magnetism. Saunders **2** (1966)
37. H.L. Zhuang, Y. Xie, P. Kent, P. Ganesh, Phys. Rev. B **92**, 035407 (2015)